The Astrophysical Journal, 722:1216–1225, 2010 October 20 doi:10.1088/0004-637X/722/2/1216

XMM-NEWTON OBSERVATIONS OF HD 189733 DURING PLANETARY TRANSITS

I. Pillitteri[1], S. J. Wolk[1], O. Cohen[1], V. Kashyap[1], H. Knutson[1,2], C. M. Lisse[3], and G. W. Henry[4]
[1] SAO-Harvard Center for Astrophysics, 60 Garden St., Cambridge, MA 02139, USA; ipillitteri@cfa.harvard.edu
[2] Department of Astronomy, University of California, Berkeley, 601 Campbell Hall, Berkeley, CA 94720, USA
[3] Planetary Exploration Group, Space Department, Johns Hopkins University Applied Physics Laboratory, 11100 Johns Hopkins Rd., Laurel, MD 20723, USA
[4] Tennessee State University, Center of Excellence in Information Systems, 3500 John A. Merritt Blvd., P.O. Box 9501, Nashville, TN 37209, USA
Received 2010 February 16; accepted 2010 August 20; published 2010 September 28

ABSTRACT

We report on two *XMM-Newton* observations of the planetary host star HD 189733. The system has a close in planet and it can potentially affect the coronal structure via interactions with the magnetosphere. We have obtained X-ray spectra and light curves from EPIC and the Reflection Grating Spectrometer on board *XMM-Newton* which we have analyzed and interpreted. We reduced X-ray data from the primary transit and secondary eclipse that occurred on 2007 April 17 and 2009 May 18, respectively. In the 2007 April observation, only variability due to weak flares is recognized. In 2009 HD 189733 exhibited an X-ray flux that was always larger than in the 2007 observation. The average flux in 2009 was higher than in the 2007 observation by a factor of 45%. During the 2009 secondary eclipse we observed a significant softening of the X-ray spectrum at a level of $\sim 3\sigma$. Furthermore, we observed the most intense flare recorded at either epoch. This flare occurred 3 ks after the end of the eclipse. The flare decay shows several minor ignitions perhaps linked to the main event and hinting at secondary loops that are triggered by the main loop. Magnetohydrodynamic (MHD) simulations show that the magnetic interaction between planet and star enhances the density and the magnetic field in a region between the planet and the star because of their relative orbital/rotation motion. X-ray observations and model predictions are globally found in agreement, despite the quite simple MHD model and the lack of precise estimate of parameters including the alignment and the intensity of stellar and planetary magnetic fields. Future observations should confirm or disprove this hypothesis, by determining whether flares are systematically recurring in the light curve at the same planetary phase.

Key words: planetary systems – stars: activity – stars: individual (HD 189733) – stars: magnetic field

Online-only material: color figures

1. INTRODUCTION

Recent work indicates that exoplanets, and especially Jupiter class planets at a distance $\lesssim 0.1$ AU from their parent stars (the so-called hot Jupiters), are in a unique X-ray environment and the effects of stellar X-rays may be significant to their evolution. The X-rays have been cited as the cause of excess heating of the planet, which can induce mass loss (Lammer et al. 2003). Further, it has been argued that the magnetic fields of the star and the planet can interact when the latter is orbiting at a distance of very few stellar radii as in the case of HD 189733 (Lanza 2008, 2009; Cohen et al. 2009). The complex magnetosphere that is formed by the star+planet system can drag material from the outer atmosphere of the planet and funnel it onto the stellar surface. The accretion of gas on the star that eventually could arise from this phenomenon can provoke shocks that heats the plasma up to a few millions of degrees and thus emits in X-rays. Furthermore, the enhanced magnetic field near the stellar surface can form very active regions on the star increasing the activity of the star in the X-ray band. Recent statistical analysis of X-ray activity of stars possessing hot Jupiters indicates that stars with close orbiting planets show enhanced X-ray emission (Kashyap et al. 2008). In the optical band, Shkolnik et al. (2003) have detected enhanced activity of Ca H and K in phase with the planet's orbital period in HD 179949.

A typical "hot Jupiter" receives $\sim 2 \times 10^4$ times more radiation from its star than Jupiter does from the Sun, and orbits at a distance of only ~ 10 stellar radii. Unlike solar system planets, where residual heat from formation and gravitational settling still plays an important part in the energy budgets of Jupiter and other giant planets, the energy budget for hot Jupiters is completely dominated by the strong radiation that they receive from their parent stars. This energy budget is poorly constrained in the X-ray and UV regimes by standard stellar atmosphere models. Thus, understanding the nature of this input and the planet–star interactions is essential for understanding the properties and the evolution of these planets. As pointed out by Lammer et al. (2003), the stellar X-ray and UV fluxes in their irradiance calculations strongly determine the amount of losses of gas from the outer atmospheres of close-in exoplanets, otherwise the losses of volatiles in models neglecting UV/X-ray irradiation are proved to be unrealistically low. The UV/X-ray flux from the star plays a crucial role in determining the photochemistry of the planet's upper atmosphere. The photochemical products can act, in turn, as high-altitude absorbers, create thermal inversions, and otherwise alter the observable properties of the planet's upper atmosphere. These effects are important when observing at lower energies/longer wavelengths (Burrows et al. 2008; Liang et al. 2004)

HD 189733 (R.A. $20^{\rm h}00^{\rm m}43\overset{\rm s}{.}7$, decl. $+22^{\rm d}42^{\rm m}39\overset{\rm s}{.}1$) is a K 1.5V type star at a distance of 19.3 pc, of mass 0.81 $M_\odot$, radius 0.76 $R_\odot$, and a rotational period of ~ 11.95 d (Henry & Winn 2008). It is in a wide binary system, and HD 189733B, the other stellar member of the binary system, is a M4V type star (with range: M3.5–M5, $M \sim 0.2\,M_\odot$; Bakos et al. 2006) orbiting at a mean distance of ~ 220 AU ($12\overset{''}{.}3$ apparent separation) with a period of 3200 yr in a plane nearly perpendicular to the Earth–HD 189733A line of sight. It is thought that the age of this system is greater than or equal to 0.6 Gyr (Melo et al. 2006). The magnetic field is estimated of a few tens of gauss, a toroidal component and higher multipole components are presumed, and

a strong shear of field lines due to differential rotation is inferred (Moutou et al. 2007).

HD 189733A hosts a Jupiter size planet (HD 189733b, $M \sim 1.15\,M_{\rm Jup}$, $R \sim 1.26 R_{\rm jup}$) at a distance of only 0.031 AU (8.75 stellar radii) and with an orbital period of 2.219 d (Bouchy et al. 2005), much lower than the stellar rotational period. HD 189733b is thus classified as a hot Jupiter planet type. The orbit is nearly circular and the orbital plane is parallel within a few degrees of the Earth-primary line of sight. This system has been the subject of many studies since its discovery, given its close distance and favorable geometry. Given Q values for giant planets in the solar system, it is thought that orbital radii of a few hundredths of an AU from parent star reduces hot Jupiters' tidal dissipation timescales to a few Myr, and tidally locked hot Jupiters should be the norm. Under this hypothesis, HD 189733b should show a pronounced temperature difference between the dayside and the nightside hemispheres. Instead, Knutson (2007) found only a modest difference of temperature between dayside and nightside hemispheres, suggesting that the thermal energy transport and thermalization in the planet's atmosphere are quite efficient. The same study shows that a bright spot is present in the planet surface displaced by $16 \pm 6^\circ$ east longitude with respect to the sub-stellar point.

Observations with the Advanced Camera for Surveys (ACS) camera on board *Hubble Space Telescope* allowed Pont et al. (2007) to infer that planet transits cover spots on the stellar surface with sizes of the order of 80,000 km. HD 189733A is known to be an active and variable K-type star with strong magnetic activity, as inferred from Ca II H&K lines (Moutou et al. 2007). Through modeling the observed Rossiter–McLaughlin effect (the apparent Doppler shift occurring for the transit of the planet at the stellar limbs) Winn et al. (2006) find that the spin stellar axis and the orbit normal are misaligned of only $1\overset{\circ}{.}4$, hinting that migration of the planets does not change this alignment.

Due to its close distance and the favorable orientation of the planetary orbit plane, HD 189733 is an ideal laboratory for the study of close in planets. Among the plethora of known exoplanets, the details on the atmosphere of HD 189733b obtained through optical and IR spectroscopy are unique.

In this paper, we report on two observations of the HD 189733 system obtained in the X-ray band with the *XMM-Newton* satellite at the time of a planetary transit and a secondary eclipse, respectively. X-ray observations can constrain model predictions, reduce degeneracy in their parameter space, and help magnetohydrodynamic (MHD) simulations to infer physical and geometrical properties of the complex magnetosphere created by star and planet.

The structure of the paper is as follows: in Section 2, we describe the observations and the data analysis, in Sections 3 and 4, we show the results and discuss them, and in Section 5, we present our conclusions.

2. OBSERVATIONS AND DATA ANALYSIS

We have obtained an observation of HD 189733 with *XMM-Newton* during the eclipse of the planet (secondary transit, when the planet passes behind the star as seen from the Earth) that occurred on 2009 May 18–19 (Obs. 0600970201). We have also analyzed a previous *XMM-Newton* archival observation of HD 189733 during the planetary transit of 2007 April 17 (Obs. 0506070201, P.I. P. Wheatley). A source close to HD 189733 is visible in both observations, especially in 2007, while the M-type companion HD 189733B is undetected. Obviously, the planet is not resolved. Figure 1 shows the EPIC images of HD 189733 obtained in 2007 (top row) and 2009 (bottom row), respectively. The *XMM-Newton Observation Data Files* of both observations were processed with *SAS* (ver. 8.0) to obtain event tables of MOS1, MOS2, and PN calibrated both in energy and position. We restricted the analysis to events in the 0.3–8.0 keV energy band and to events that triggered at most two adjacent pixels as suggested by the *SAS* guide. We have extracted events of HD 189733A from a circular region that avoids the contamination from the M star companion HD 189733B. From the events selected in this region, we have obtained light curves (Figure 2) and EPIC spectra of HD 189733A. For the analysis of light curves and spectra we focus primarily on the PN data in this work because of its higher efficiency in collecting counts with respect to both MOS cameras (4557 PN counts versus 1166 MOS1 and 1190 MOS2 counts in the source extraction region, respectively). A likely loss of data telemetry causes a dip at ∼23 ks with a duration of ∼900 s in the light curves of 2009 observation, more marked in the PN data.

In order to characterize the variations of the source at short timescales, we consider the pulse invariant (PI) spectrum of PN events in a moving window comprised of 200 events. We compute the average energy of the spectral distribution, as well as the median, the standard deviation, and the 16% and 84% quantiles for a contiguous set of 200 photons (see Figure 3). The window is moved by adding five events at the end and removing five from the beginning. We obtain a smoothed light curve in the same manner, with the time interval between the first and last events in the window suitably corrected for the presence of gaps in the exposure time. A background is estimated for each interval and is subtracted from the light curve.[5]

We have also extracted Reflection Grating Spectrometer (RGS) spectra to have a higher resolution spectrum ($\delta\lambda \sim 0.04$ Å) in order to observe the behavior of features, especially the O VII triplet and its changes during the observation. The ratio of forbidden to recombination lines from the O VII triplet offers a diagnostic of the plasma density. For the main flare observed in the light curve of 2009 observation, we have performed time resolved spectroscopy of the PN data by considering the spectrum during the flare, as well as before and after the flare. The spectra of EPIC PN have been analyzed with XSPEC software to obtain best-fit parameters from thermal models (APEC) with one or two temperatures. Given that absorption is very low due to the short distance to the star, we have considered only unabsorbed spectral models. The free parameters were the temperatures, the global abundance, and the emission measures.

3. RESULTS

In Figure 2 we plot the light curves from the 2007 and 2009 observations in three bands: 0.3–0.8 keV (red), 0.3–2.5 keV (blue), and 0.3–8.0 keV (black). The background curve is shown in gray. The duration of the planetary transit and the secondary eclipse is ∼108 minutes from 1st to 4th contact, i.e., 6480 s.

The 2007 light curve shows a modest flare in coincidence of the planetary transit as the spectrum seems to harden at ∼30 ks ($\phi \sim 0$) and decays exponentially post-transit. We find that a 1T thermal model with plasma temperature of ∼0.6 keV reasonably fits the spectrum during the first flare. This is the most prominent feature in the 2007 light curve.

[5] Note that background is ignored for the spectral distribution both due to the relative constancy of the background spectrum and the numerically small correction to the spectrum; see Figure 2.

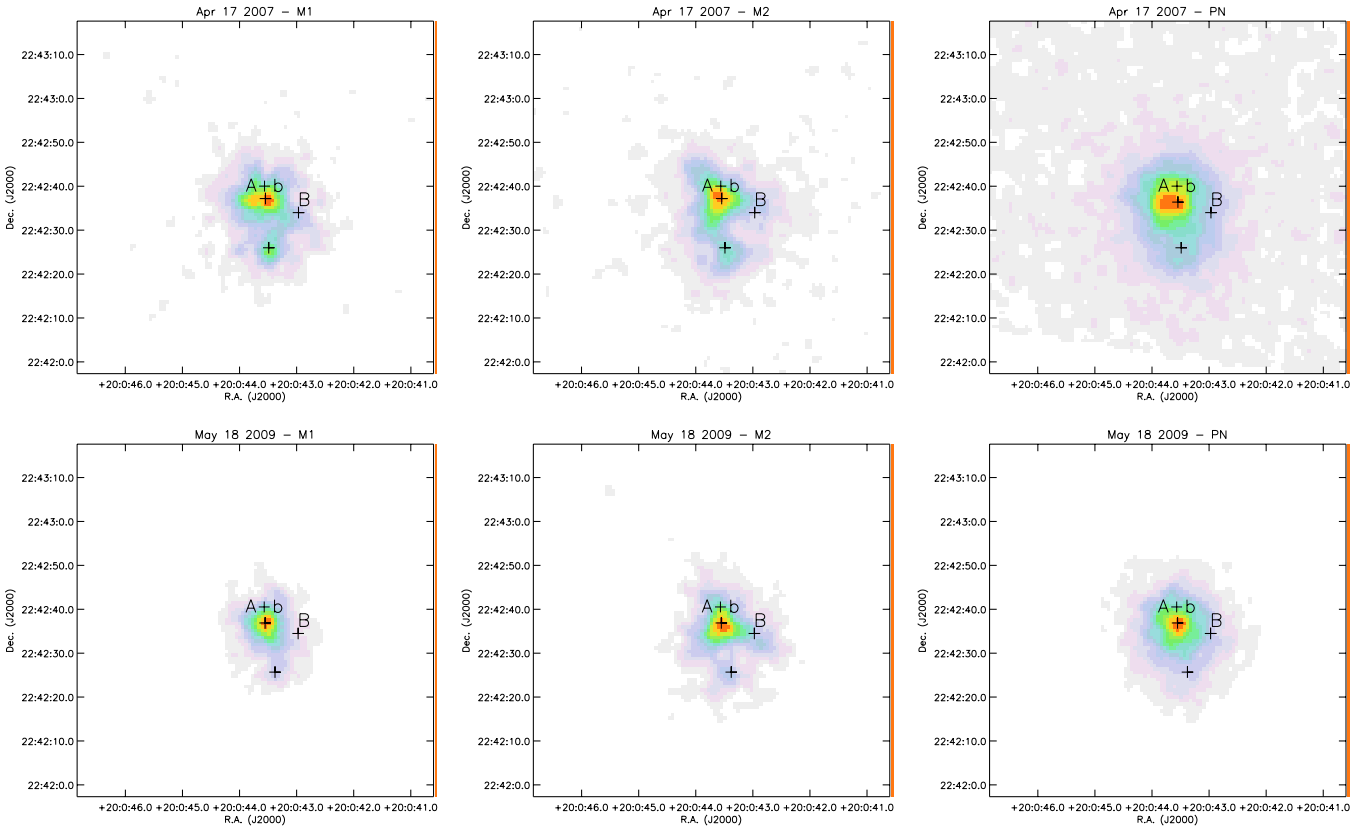

Figure 1. EPIC images of HD 189733A+B observed with *XMM-Newton* in 2007 April (top row) and 2009 May (bottom row). Images of MOS 1, MOS 2, and PN are shown in sequence from left to right. The companion HD 189733B is not visible in both observations. A bright source with uncertain optical counterpart is visible to the south of HD 189733A and it has faded in 2009.

(A color version of this figure is available in the online journal.)

Table 1
Best-fit Parameters of Spectra Collected During the Observations in 2007 and 2009

Dates	kT 1	E.M. 1	kT 2	E.M. 2	$\chi^2_{\rm red}$	$P(\chi^2 > \chi^2_0)$	Flux	Notes
	keV	10^{51} cm^{-3}	keV	10^{51} cm^{-3}			10^{-13} erg s^{-1} cm^{-2}	
2007	$0.57^{0.59}_{0.51}$	$0.95^{1.26}_{0.76}$	$0.24^{0.25}_{0.16}$	$0.90^{1.13}_{0.73}$	1.13	0.14	2.50	Whole obs.
2007	$0.59^{0.65}_{0.48}$	$2.50^{3.00}_{1.98}$	···	···	1.45	0.07	3.14	First flare
2007	$0.56^{0.59}_{0.48}$	$0.95^{1.40}_{0.76}$	$0.24^{0.27}_{0.18}$	$0.97^{1.21}_{0.64}$	1.16	0.08	2.50	No first flare
2009	$0.42^{0.46}_{0.40}$	$2.81^{3.15}_{2.46}$	···	···	1.29	0.04	3.11	Pre-flare
2009	$0.61^{0.63}_{0.57}$	$3.15^{3.51}_{2.79}$	···	···	1.37	0.02	4.38	Flare
2009	$0.50^{0.53}_{0.46}$	$3.22^{3.63}_{2.83}$	···	···	0.87	0.78	3.72	Post-flare
2009	$0.86^{1.02}_{0.77}$	$0.32^{0.64}_{0}$	···	···	1.1	0.25	1.19	Flare–pre-flare

Note. For 2009 we list the results of the three time intervals: before the flare, during the flare, and after the flare.

The remaining part of the observation is best modeled with a 2T thermal model with a cool component ($kT = 0.24$ keV) and a hot component ($kT = 0.56$ keV) very similar to the first flare temperature. The unabsorbed flux in the 0.3–8 keV band energy is $\sim 2.5 \times 10^{-13}$ erg s^{-1} cm^{-2} for a luminosity of $L_X = 1.1 \times 10^{28}$ erg s^{-1}. Table 1 shows the results of the fits. Abundances are found at $Z \sim 0.15$–$0.2\ Z_\odot$, as in active stellar coronae and very young stars (Maggio et al. 2007). The PN rate is on average $\sim$65 counts ks^{-1} during most of the observation, reaching a peak of $\sim$95 counts ks^{-1} during the first flare.

During the 2009 observation, the star had an X-ray activity more pronounced than in 2007. The mean energy of the 2009 spectrum is $\sim$700 keV. In 2009, the PN rate of HD 189733A is always larger than in 2007: the lowest rate is in fact $\sim$95 counts ks^{-1} in 2009 with a peak of $\sim$350 counts ks^{-1} (see Figure 3).

During the secondary eclipse, the light curve shows a *softening* of the spectrum. From Figure 3 we see that the mean of the PN distribution of PI gets softer during the eclipse. The mean photon energy in the 0.3–1.5 keV range before and after the eclipse is $\sim 700 \pm 10$ (1σ), while during the middle of the eclipse it is $\sim 660 \pm 10$ eV (1σ); thus, it is significant at a level of $3 \sim \sigma$. During the eclipse the rate increases. The quartile curves show that the soft part of the spectrum increases while the hard part of the spectrum decreases.

The light curves in Figures 2 and 3 show a flare with a decay of $\sim$10 ks that occurs 3 ks after the end of the planetary eclipse. The flare decay is characterized by several smaller impulses after

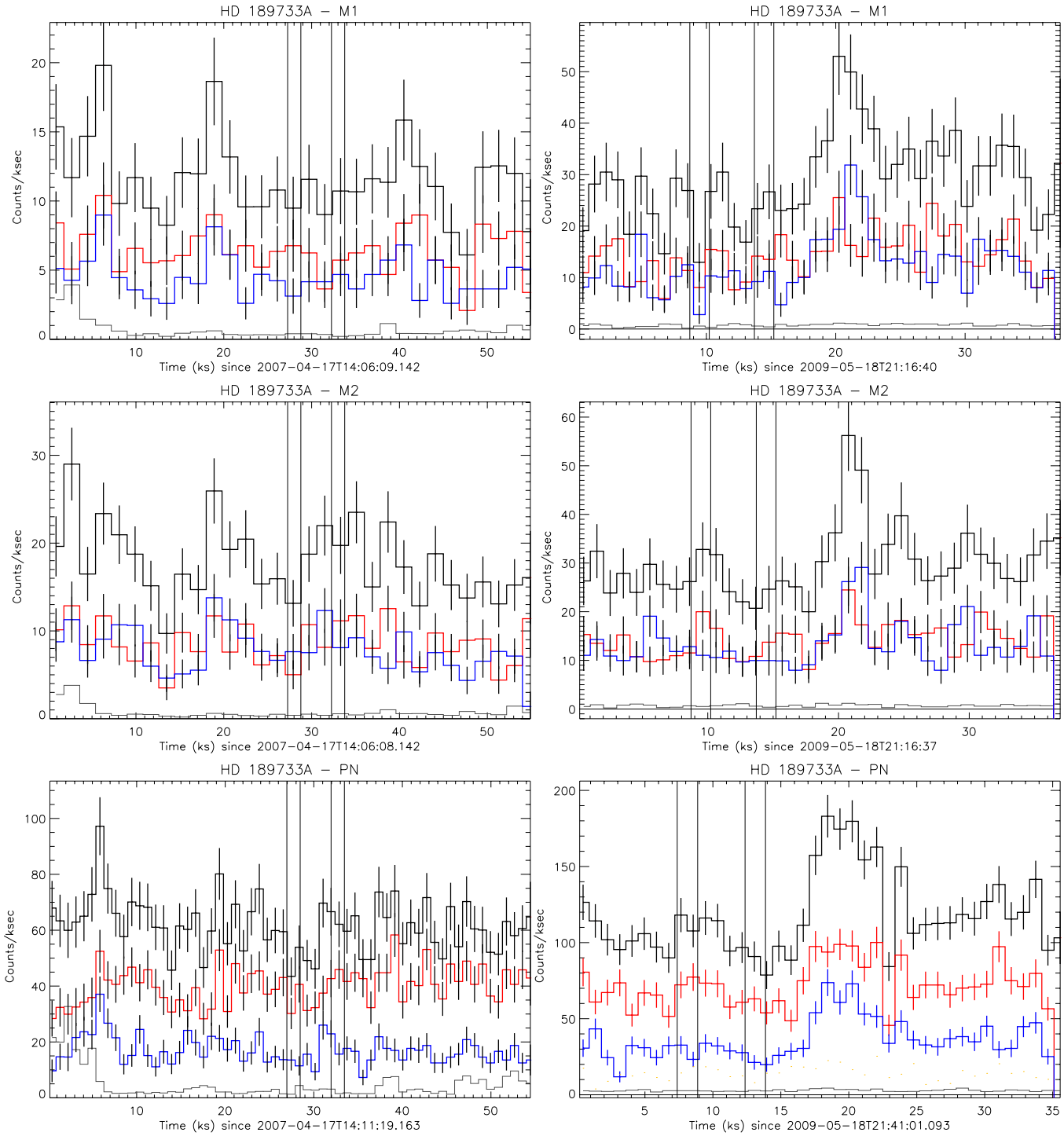

Figure 2. Light curves of HD 189733. On the left column: light curves of MOS1, MOS2, and PN acquired during the 2007 observation. On the right column, the same for the 2009 observation. Error bars are at 1σ level. The red light curve is in the 0.3–0.8 keV energy band while the blue light curve is in the 0.8–2.5 keV energy band. Gray curve is the background. Bin size is 900 s for PN and 1800 s for MOS 1 and 2.

(A color version of this figure is available in the online journal.)

the main ignition.[6] The flare phase is $\phi \sim 0.54$ which would correspond to the planet being 16° past the Earth–star line of sight (see Figure 4). In the soft band (0.3–0.8 keV), the light curve of PN has a step-like profile (Figure 2), characterized by an almost flat high level, whereas in MOS 1 and 2 the soft band light curves show a more usual peaked profile. The difference of the flare profile in PN and MOS is very likely due to their different responses at low energies with the PN being more sensitive to low energies than MOS.[7] The plasma spectrum becomes hard at the flare peak as shown by the median and quartile curves (right panel in Figure 3). We deduce that the temperature of the plasma increases approaching the peak.

[6] A likely loss of telemetry is causing the sharp dip in the decay around 23 ks.

[7] The ratio of normalized PN and MOS effective areas shows that PN is proportionally more sensitive than MOS by a factor ∼2 in the range 0.3–0.7 keV.

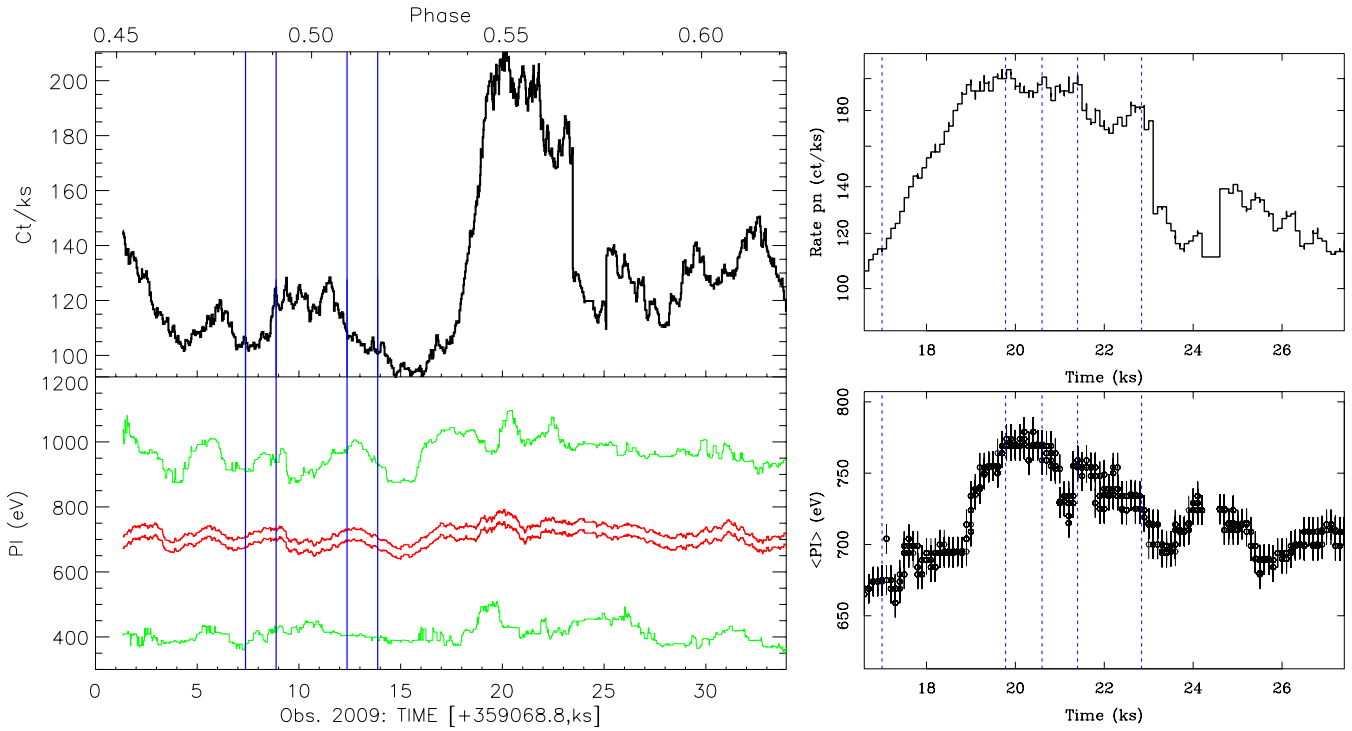

Figure 3. Intensity (top panels) and spectral variation (bottom panels) of HD 189733A during 2009 (secondary eclipse) registered from PN. In the left panels are the curves relative to the whole exposure time. Vertical lines denote the 1st, 2nd, 3rd, and 4th contact. In the bottom left panel, the green curves represent the 16% and 84% quantiles of the distribution of a sample of 200 photons, and show the overall width of the PI spectral distribution. Red curves represent the mean $\pm 1\sigma$ standard deviation of the mean of the sample of PI between 0.3 and 1.5 keV, and show the temporal variation of the spectrum. In the right panels, we plot the rate and the mean of PI during the flare with a log scale in the *y*-axis of rate. Vertical lines denote the beginning of the flare, the peak, and three secondary impulses.

(A color version of this figure is available in the online journal.)

To investigate the characteristics of the flare we have analyzed the PN spectra in the intervals 0–15 ks, 15–25 ks, and 25–35 ks (chosen by visual inspection of the light curve). In Table 1, we report the best-fit parameters and 90% confidence ranges of the model fit to the spectra in the three phases. We also list the result of fitting the flare spectrum subtracted from the pre-flare spectrum.

The flare spectrum in 2009 shows a modest increase in temperature, changing from ∼0.4 keV prior to the event to ∼0.9 keV (flare spectrum minus pre-flare spectrum). The temperature of the flare is similar to that observed in solar flares (∼10 MK). The total flux of HD 189733A+b increases by a factor of 85% and the emission measure by 11%. The flux in the 0.3–8 keV band due to the flare is 1.3×10^{-13} erg s^{-1} cm^{-2}. Some features of the coronal spectrum are enhanced during the brightening. Figure 5 shows the PN spectra in the three phases: black is pre-flare, red is the flare, and blue is after the flare. The most notable difference is around 0.57 keV or 22 Å where the O VII triplet is located (recombination: $r = 21.62$ Å, intercombination: $i = 21.84$ Å, forbidden: $f = 22.10$ Å). This region of the spectrum remains in excess at a level of $\sim 2\sigma$ with respect to the best-fit thermal model.

We explore this spectral region in detail by means of the RGS 1 spectrum that allows a much higher resolution with respect to the EPIC cameras in order to distinguish between the *r*, *i*, and *f* triplet lines of O VII. The relative intensity of these lines offers a diagnostic of the plasma density, wherein the forbidden line is formed when the plasma has low density and the corresponding energetic level is depopulated by collisions under increasing plasma density. Figure 6 shows the spectra in the three phases as above. We have rebinned the spectra, by decreasing the

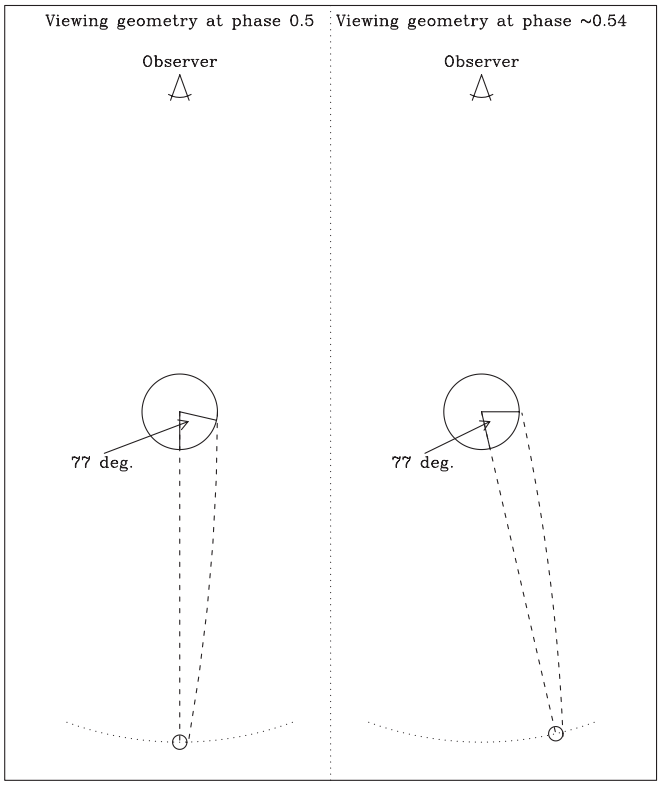

Figure 4. Scheme of the angle between sub-planetary point and active region where the large flare could have occurred in 2009.

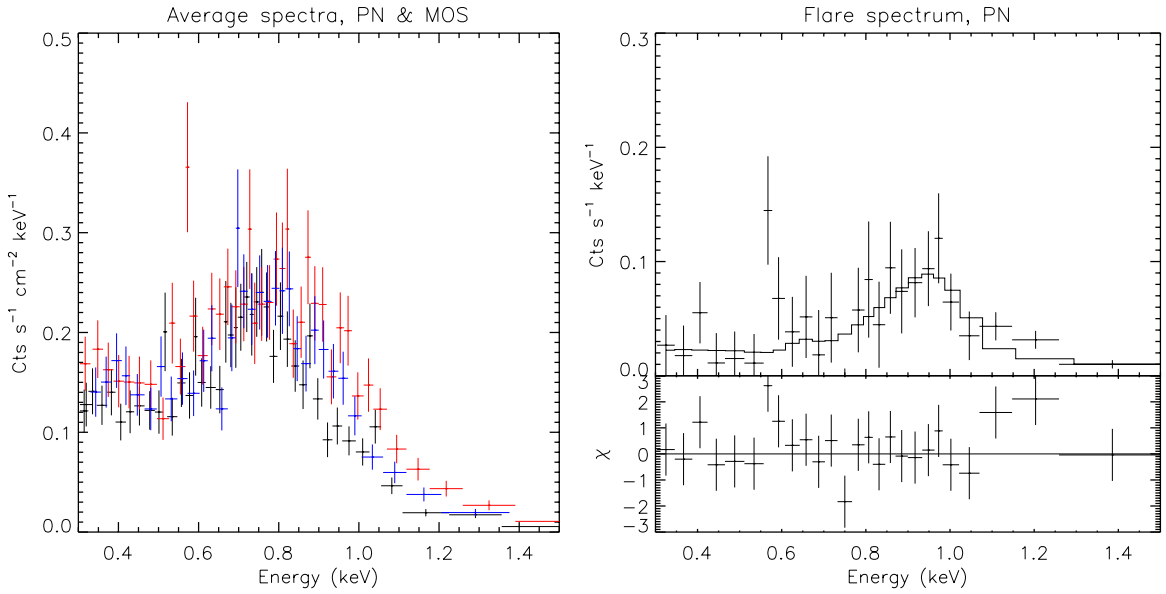

Figure 5. Left panel: PN spectra of HD 189733 A during the three phases, pre-flare (0–15 ks, black), flare (15–25 ks, red), and post-flare (25–35 ks, blue). Right panel: flare spectrum (minus pre-flare spectrum) with best-fit model and residuals. The region of O VII at ∼0.57 keV (∼22 Å) is enhanced during the flare.
(A color version of this figure is available in the online journal.)

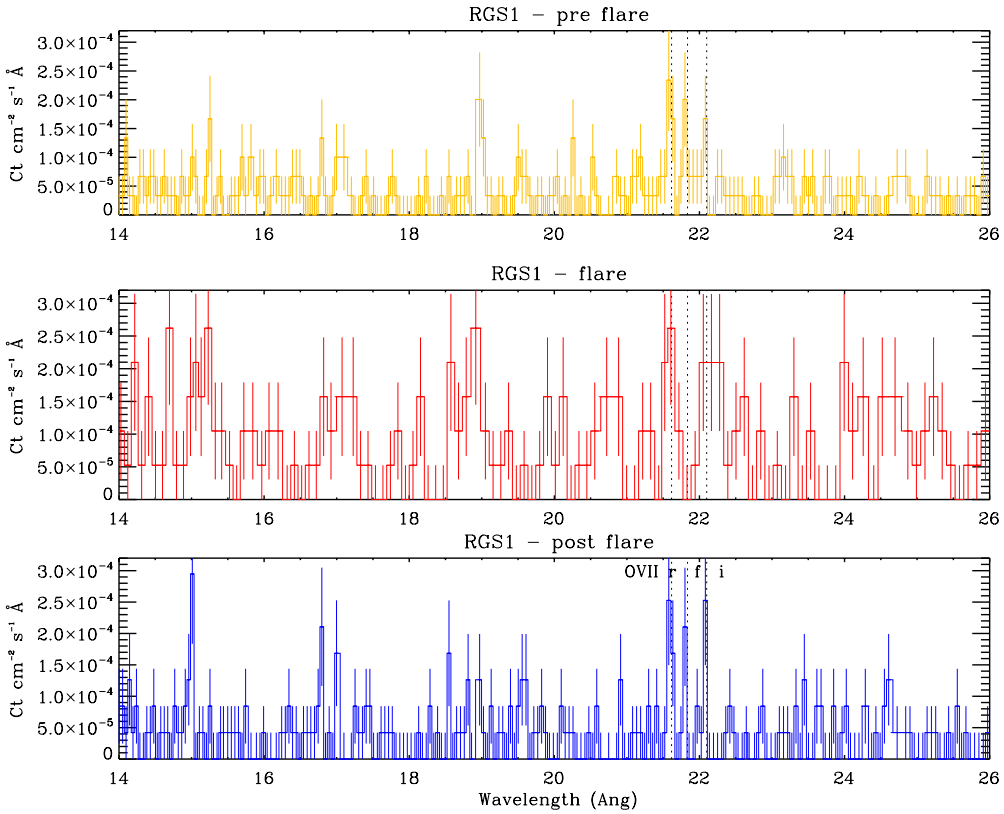

Figure 6. RGS 1 spectra of HD 189733A during the three phases: pre-flare (0–15 ks), flare (15–25 ks), and post-flare (25–35 ks).
(A color version of this figure is available in the online journal.)

instrumental resolution by a factor of 5 to enhance the signal. In these spectra, we can easily distinguish between *r*, *i*, and *f* lines. During the flare the *i* line seems to disappear and the *f* line is less luminous. After the flare the *f* line remains quite luminous and this fact suggests that low density plasma continues to be visible after the heating. There are indications that the *r* recombination line is shifted by $\gtrsim$150 km s^{-1}, which is consistent with the orbital speed of the planet (∼150 km s^{-1}). Linsky et al. (2010) looked for UV signatures of ionized gas co-orbiting with HD 209458b; while they found evidence of an exosphere, they concluded that higher signal-to-noise ratios (S/Ns) were needed to ascertain the velocity structure. Likewise, our data are not sufficient for such detection. Other visible changes during the flare which may be related to the increase of temperature are an enhancement of the O VIII line at 18.96 Å, the Fe XVII lines at 15 Å and 17 Å, and an enhancement of the continuum level.

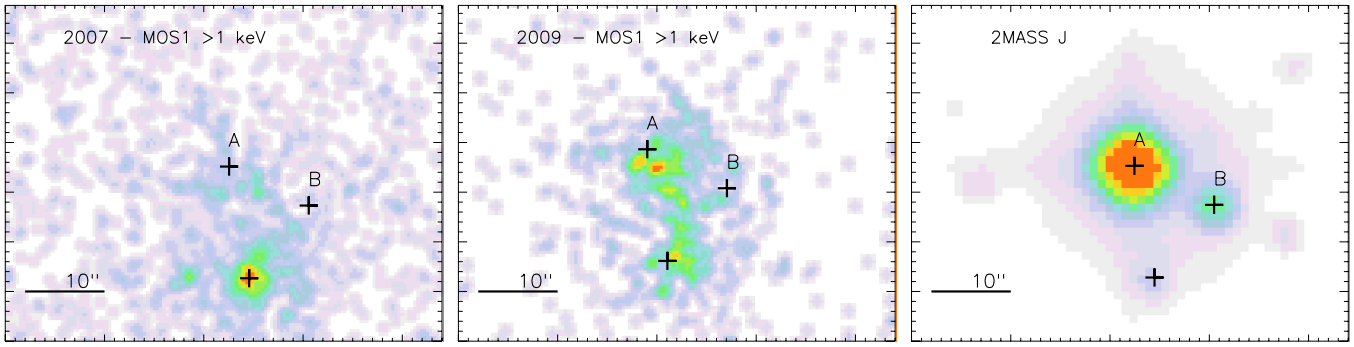

Figure 7. EPIC and 2MASS images of the X-ray source at ∼12″ from HD 189733. From left to right: MOS1 > 1 keV in 2007, MOS 1 > 1 keV in 2009, 2MASS *J*-band image. Positions of HD 189733A, HD 189733B, and the source are indicated by crosses.

(A color version of this figure is available in the online journal.)

In the framework of modeling of the flares in the stars in analogy with solar flares, several studies have been done involving both simple models based on scaling laws and more detailed MHD simulations (see Reale 2007, and references therein). A simple model for the flare is given by a loop formed by the magnetic field in which the plasma is constrained to move only along the field lines. The heating of the flare is provided at some point of the loop, which usually has an aspect ratio (base radius on loop semi-length) of $r/L = 0.1$ similar to loops observed on the Sun. If the flare we observed took place in a coronal loop anchored to the star surface, a rough estimate of the semi-length of the loop is provided by the formula given by Serio et al. (1991). We obtain a semi-length of the order of ∼75% $R_\star$ or 4×10^{10} cm (Serio et al. 1991; Reale et al. 1997), assuming a peak temperature of 0.86 keV and no further heating mechanism at work after the initial loop heating. Given that we cannot estimate the true peak temperature, the size we would have derived is a lower limit. We can suppose that the size of the flaring loop is of the order of the stellar radius. Loops of the order of the stellar radius are also inferred from a detailed modeling of a large flare observed in the very active dM star Proxima Centauri (Reale et al. 2004). Given the proximity of the planet (at d ∼ 8.75 $R_\star$), the perturbation on the stellar magnetic field due to the planet could affect the formation of loops and their evolution. The unusual flaring volume suggests that the site of the flare should be an extended region of the corona or an arcade formed of similar loops. From the estimates of the emission measure and the volume we derive a mean electron density in the plasma of $n_e \sim 9 \times 10^9$ cm^{-3}.

From the rotational period ($P = 11.95$ d; Henry & Winn 2008) and stellar radius ($R = 0.76\ R_\star$; Pont et al. 2007) we infer a mean rotational velocity of $v_{\rm rot} = 3.4$ km s^{-1}. Early studies of main sequence solar type stars have shown that the X-ray luminosity is well correlated with rotational velocity (Pallavicini et al. 1981), given the link between rotation, dynamo efficiency, coronal magnetic field, X-ray activity, and L_X. Comparing with the Sun, we see that L_X and $v_{\rm rot}$ scale reasonably well with the $L_X \sim (v \sin i)^2$ law in the non-saturated regime of L_X. From the rotational velocity ratio between HD 189733A and the Sun (2 km s^{-1}) a mean magnetic field strength ∼1.7 times the mean solar field is inferred.

The M-type companion is not detected in either observations, although it could have been resolved given the separation of ∼12″. We have estimated an upper limit to its X-ray luminosity in 0.3–8.0 keV band of $L_X \leqslant 9 \times 10^{26}$ erg s^{-1}. The non-detection of this star has some implications for the estimate of the age of the system as we will discuss in Section 4.

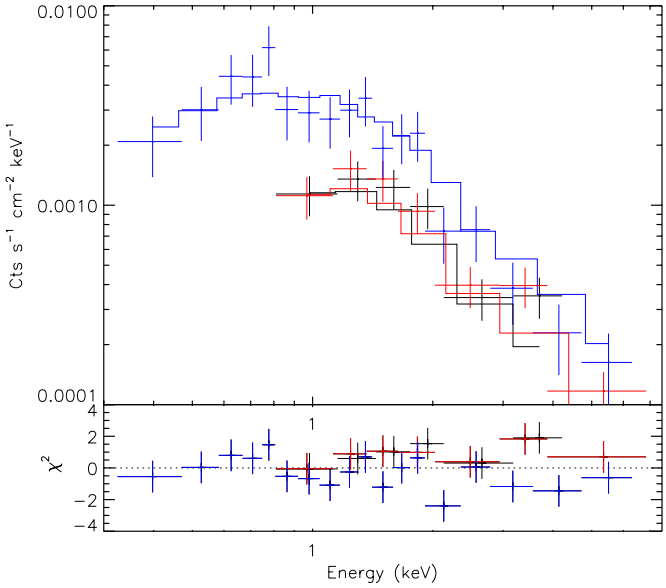

Figure 8. PN and MOS spectra of the X-ray source at ∼12″ from HD 189733 obtained during the 2007 observation. The best-fit model is an absorbed APEC thermal model.

(A color version of this figure is available in the online journal.)

3.1. The X-ray Source Near HD 189733

The X-ray images in 2007 and 2009 show a source ∼12″ to the south of HD 189733A. The source is brighter in 2007 than in 2009 (see Figure 7). The spectra obtained in 2007 are shown in Figure 8, those from the 2009 observation have poorer statistics and are not shown here. The source reveals a quite hard spectrum and, given that HD 189733A has a quite soft spectrum, the contamination from this source to HD 189733A spectrum is negligible. We have tried best fit with models composed by an absorbed power law and an absorbed APEC thermal model. In both cases, the absorption is high: $N_{\rm H} \sim 1.4 \times 10^{21}$ cm^{-2}. Given that the spectra from 2009 have poor statistics, a simple model with an absorbed power law of index of ∼1.7 has a good agreement with the data. On the other hand, the spectra of 2007 have better statistics and the shape reveals some features around 1 keV, so the simple power law is not appropriate. When modeled with an APEC thermal component, we find a high plasma temperature value of the order of 8 keV. The flux in 0.3–8.0 keV band is 1.9×10^{-13} erg s^{-1} cm^{-2} in 2007, whereas it is 1.4×10^{-13} erg s^{-1} cm^{-2} in 2009. The nearest optical/infrared counterpart to this X-ray source is an object in

the Two Micron All Sky Survey (2MASS; Cutri et al. 2003) and NOMAD (Zacharias et al. 2005) catalogs at $\sim 3''$. It has a poorly determined 2MASS photometry given the proximity to HD 189733 and quite large proper motions that hint that the cataloged object should be quite close. On the other hand, the value of absorption of the X-ray spectrum of this source suggests that it should be quite distant from the Sun but still inside the Galaxy. In fact, typical values for the total $N_{\rm H}$ column in the direction of HD 189733 are between 3.8×10^{21} cm^{-2} and 3.9×10^{21} cm^{-2} (Kalberla et al. 2005; Dickey & Lockman 1990). By considering the flux in 2007 and 2009, and placing it at a distance of 1000 pc the luminosity yields $\log L_X = 31.2$–31.4.

4. DISCUSSION

In this paper, we have analyzed two X-ray observations of HD 189733A: the first obtained during a planetary transit on 2007 April 17 and the second during a planetary eclipse that occurred on 2009 May 18. Here, we discuss the features observed in the light curve of 2009 and we relate them to possible effects of interaction of the planet and the host star.

4.1. Observed Features

The first feature we have observed in 2009 is a *softening* of the emission during the planet eclipse at a level of $\gtrsim 3\sigma$. Although similar variations of the spectrum hardness are seen in the light curve, this softening has a direct correspondence with the eclipse timing and, in addiction, during the eclipse the star has the softest emission ever recorded in both the 2007 and 2009 observations. The mean PI in EPIC–PN in the 0.3–1.5 keV band is 700 ± 10 eV before the eclipse and after the flare that occurred post-eclipse, while it is 660 ± 10 eV at the mid eclipse.

An analogy between HD 189733b and Jupiter here may be appropriate. Jupiter shows enhanced soft emission in X-rays coming from the equatorial region and due to the interaction of solar X-rays with the upper atmosphere of the planet (Branduardi-Raymont et al. 2007). Furthermore, a harder X-ray emission is detected near the poles of Jupiter and may be due to charge exchange mechanisms caused by precipitating ions of carbon, sulfur, and oxygen (Hui et al. 2009; Branduardi-Raymont et al. 2007). The flux in 0.2–7 keV coming from Jupiter aurorae is $\sim 7 \times 10^{-14}$ erg s^{-1} cm^{-2} that corresponds to a luminosity of $\sim 5 \times 10^{15}$ erg s^{-1}. By using simple scaling, taking into account the star–planet distance in HD 189733, the higher luminosity of the star with respect to the Sun ($10 \times L_{X,\odot}$) and the distance to HD 189733, we estimate that the power emitted by aurorae would be $L_{X,\rm aur} \sim 1.4 \times 10^{21}$ erg s^{-1}, corresponding to a flux to Earth of $f_{X,\rm aur} \sim 3 \times 10^{-20}$, which is too faint to be detected by *XMM-Newton*, unless there are additional sources of energy caused by the magnetic field topology. If the softening is related to the secondary eclipse, it cannot be related to a scaled emission of Jupiter for the case of HD 189733b. With only one observation, we are not in a position to assess that the softening is related to the secondary eclipse. A series of observations at the same phase would reveal if the softening is systematically recurrent.

The second relevant feature present in the light curve of 2009 is the most intense flare recorded in both observations, occurring ~ 3 ks after the secondary eclipse. The increase of flux is equal to $\sim 85\%$ of the emission before the eclipse and the plasma temperature shows a modest heating passing from ~ 0.4 keV prior to the event to ~ 0.9 keV. The properties of the flare like temperature, luminosity, and decay rate are similar to other flares observed in solar type stars without hot Jupiters. During the flare, the lines of O VII at ~ 22 Å are more luminous than before and after the event. The O VII complex remains in excess with respect to the best-fit model of the flare spectrum. High-resolution RGS spectra show that the *f* O VII line remains quite luminous after the event and the *i* line almost disappears.

During its cooling phase, we see several impulsive events (see Figure 3). It is as though there are multiple small flares occurring as the overall structure is cooling. The faster decay time would imply loops smaller than the main flaring loop. A peculiar characteristic of the small impulses is that the rate increases while the median PI steadily decreases. One way to understand this is to imagine that the flare occurred close to the limb, and at least during the occurrence of such events the corresponding part of the corona was emerging into view. If our interpretation of this evidence is correct, then the flare is occurring on the limb when the planet is at phase approximately 0.54. This would put the flare displaced by $\sim 77^\circ$ and the meeting at the sub-planetary point (see Figure 4).

Given the timing of the flare, one could speculate that the coronal region where it took place could be displaced by $\sim 77^\circ$ and trailing the sub-planetary point. The presence of spots and active regions on the stellar surface rotating synchronously with the planet have been reported in the literature in stars with hot Jupiters. Shkolnik et al. (2003) and Shkolnik et al. (2005) report that HD 179949 and υ And show variability of chromospheric activity indicators phased with planet rotation, thus hinting that the presence of hot spots rotating synchronously with the planet is a consequence of star–planet interaction. The spots are displaced with respect to the sub-planetary point by $+70^\circ$ and -170°, respectively. Analogously to the solar corona these spots should be the chromospheric footpoints of coronal loops. Shkolnik et al. (2008) has also suggested some excess of flaring activity on HD 189733 in phase with the planet rotation superimposed to the main long lasting active regions on the stellar surface.

One speculative hypothesis is that the large flare we have observed could arise from active regions for which the activity is triggered by the complex magnetic interaction that should be present between the star and the planet. In summary, we cannot draw a conclusion on this point with only one observation. As in the case of the softening, a series of further observations around the secondary eclipse could establish the systematic recurrence of high activity just after the end of the eclipse and coming from active regions triggered by star–planet interaction.

4.2. Comparison with SPI Models

Lanza (2008) proposed an analytical model for the stellar magnetic field in the case of star-planet interaction. This model was aimed at explaining the phase shifts of active regions with respect to the sub-planetary point observed. With a suitable choice of the model parameters, the author shows that this simple model can reproduce these phase shifts for HD 189733, HD 179949, υ And, and τ Bootis. The prediction from this model for the case of HD 189733 is that a phase shift between sub-planetary point and active region should be $\sim 78^\circ$. With the same model, Lanza (2009) has addressed the energy budget, the intermittent nature of the visibility of spots, and the effect that could be seen in the radio and X-ray bands. From a qualitative point of view the stellar magnetic field should be able to drag material evaporating from the planet and to deposit it in an azimuthal flux rope in the outer part of the corona. This region should be the site of an enhanced X-ray activity due to

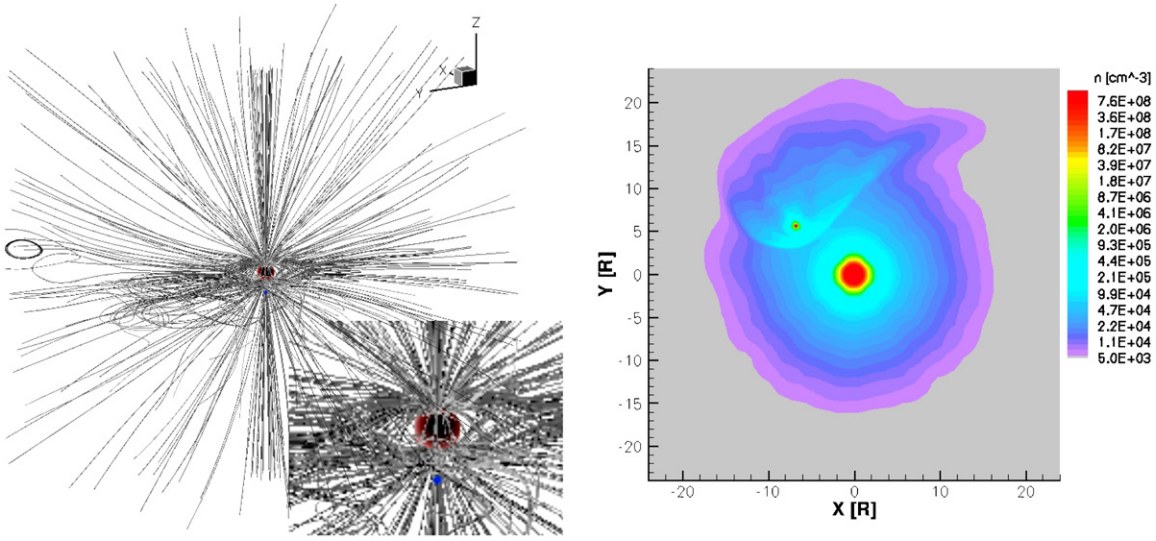

Figure 9. MHD model of the star+planet. Left panel: one frame of the MHD simulation. The star and the planet are represented by the red and blue spherical shades, respectively. Lines of the magnetic field are drawn in gray; the inset plot in the right bottom part shows the central star and the planet. Right panel: density image viewed from the top. The model predicts a denser trail orbiting synchronously with the planet.

(A color version of this figure is available in the online journal.)

magnetic reconnection (see Figure 4 for a simple schematic). By comparing our observational results to this model, we observe that the large flare in 2009 can fit consistently with this model and the excess of flaring activity suggested by Shkolnik et al. (2008) under the hypothesis that it comes from active regions displaced by ∼75°–78° with respect to the sub-planetary point.

We have carried out preliminary MHD simulations of the star+planet system within the dipolar field setup ("case A") of Cohen et al. (2009), but with the stellar and planetary parameters of the HD 189733 system. The planetary magnetic field is taken to be half that of Jupiter (with an equatorial field of 2 G); this is a reasonable assumption since tidal effects will have reduced the planetary rotation compared to that of Jupiter. Figure 9 shows one frame of the time evolution of the magnetic field of HD 189733A+b system based on our MHD simulation. The simplified dipole model produces a density enhancement in the intervening interplanetary medium that is threaded by complex magnetic fields. There is thus a greater potential to observe transients occurring in this region. The density enhancement is formed by plasma trapped into closed magnetic field lines that would have been opened in the absence of the planet interaction.

In summary, we find elements of consistency between the observed features in the X-ray band, optical chromospheric indicators, and model predictions. The magnetic interaction of planet and host star can enhance the activity in some regions of the stellar surface and these are probably among the most active regions of the star chromosphere and corona. As suggested by Shkolnik et al. (2008) based on chromospheric activity indicators, the spot activity can be enhanced or reduced due to the complex magnetic field evolution. This part of the star–planet interaction is observed as flares. On the dayside of the planet, it is plausible that the interaction manifests itself as colliding wind from the star on to the inflated atmosphere and with polar aurorae that emit X-rays harder than the main coronal emission, although this emission remains too faint to be detected.

Although our data do not allow us to draw specific conclusions, they suggest that effects of the magnetic interaction between a star and a close planet could be detected in X-rays. A series of observations in the same phase range near the secondary eclipse and perhaps coordinated with optical observations of chromospheric activity indicators could allow us to distinguish systematic effects caused by planet presence from random variability intrinsic to the coronal activity.

4.3. The Age of HD 189733 and its Activity

The age of HD 189733 has been estimated by Melo et al. (2006) to be greater than 0.6 Gyr based on indicators of chromospheric activity calibrated on normal main-sequence stars. Furthermore, these authors reported a very low abundance of Li (A(Li)< -0.1) in HD 189733A. For comparison, in the Sun A(Li) is ∼2 at an age of 4.6 Gyr. Lithium is destroyed during the main-sequence phase because of convection that brings lithium in the inner layers of the star where at a temperature of 2–3 MK it is burned. Both Li and chromospheric indicators are sensitive for ages < 0.5–1 Gyr. In the case of HD 189733, the use of chromospheric lines could be biased by the enhanced activity of the star itself and, eventually, by SPI. Our X-ray observation suggests a better constraint on its age.

The non-detection of HD 189733B, a M4 spectral type star, at a level of $L_X \leqslant 10^{27}$ erg s^{-1} suggests an age estimate of HD 189733 older than the current one. M-type stars exhibit a decay of X-ray emission during main-sequence phase slower than in G- and K-type stars due to the lower rate of dissipation of angular momentum and the link between rotation and dynamo efficiency. Feigelson et al. (2004) have studied a sample of low mass stars in the Chandra Deep Field North. In this sample, M4 stars are characterized by $L_X \sim 10^{28}$ erg s^{-1}, and the age of the sample is presumed to be greater than 3 Gyr. Given the non-detection of HD 189733B, we suggest that the age of this system could be tentatively estimated as being older than 2 Gyr.

Placing the system at an age of 2 Gyr, the X-ray luminosity of HD 189733 ($L_{X,*} \sim 10 L_{X,\mathrm{Sun}}$) fits the trend observed from studies of X-ray luminosities and activity in K-type stars of open clusters and field stars (see Giardino et al. 2008, and references therein). Mamajek & Hillenbrand (2008) consider the age estimates from various indicators like Ca H&K lines, A(Li), rotation, and X-ray emission, thus obtaining several relations between age and these observables. With a rotational period of ∼12 d and a K1-type star, HD 189733 would fit close

to the age of Hyades (Mamajek & Hillenbrand 2008, see their Figure 10). But the value of $\log R'_{\rm HK}$ reported by Melo et al. (2006) and the curves given by Mamajek & Hillenbrand (2008) in their Figure 12 would suggest an age of $\tau \geqslant 1.7$ Gyr. Furthermore, U, V, W space motion components ($U = -8.6$ km s^{-1}, $V = -14.4$ km s^{-1}, $W = 015.9$ km s^{-1}) are not compatible with those of the Hyades moving group (Montes et al. 2001). In conclusion, although the determination of the age of an isolated star can be difficult and poorly constrained, the non-detection of the M-type companion below $\log L_X \sim 27$ hints an age of HD 189733 around 1.7–2 Gyr.

5. CONCLUSIONS

In this paper, we have presented the analysis and the interpretation of X-rays, light curves, and spectra that we have acquired during a secondary eclipse of the planet HD 189733b observed in 2009 with the *XMM-Newton* satellite. For completeness we have also analyzed in a homogeneous way a previous observation taken in 2007 during a planetary transit on the same target. Our group has also carried out MHD simulations of the magnetic interaction between star and planet. From the observations we have estimated that the average X-ray flux of the star in 2009 ($f_X \sim 3.7 \times 10^{-13}$ erg s^{-1} cm^{-2}) has been 45% higher than the average flux in 2007. The light curve of 2007 shows impulsive variability which is considered quite usual for a K-type star quoted at an age of 1 Gyr. During the planetary transit, we do not observe spectral or rate variations timed with the transit.

In the light curve of the 2009 observation, we have observed a softening of the spectrum significant at a 3σ level during the secondary eclipse and the biggest flare recorded in both observations occurring 3 ks after the end of the planet eclipse. The softening is well phased with the planet eclipse. The median of the spectrum changes from an average value of 700 ± 10 eV before and after the eclipse to 650 ± 10 eV at the eclipse center. The decay phase of the main flare in the light curve shows several superimposed minor ignitions perhaps occurring in the same region where the main flare took place. We have fitted the spectrum subtracted from the pre-flare spectrum with a monothermal APEC model. The flare exhibits an average plasma temperature of 0.9 keV while the quiescent plasma temperature is around 0.5 keV. The RGS spectrum shows a variability of the relative strength of the O VII triplet lines prior, during, and after this flare. In particular, we noticed the reduction of intercombination and forbidden lines during the flare, and a bright forbidden line after the end of the flare. These two behaviors of the O VII triplet lines are explained as an increase of density in the flaring region during the ignition, and a persistent low density bright/hot plasma after the end of the flare. By using a simple model of cooling loop as in Serio et al. (1991) and Reale et al. (1997), we infer a size of the flaring region of the order of the stellar radius. From $L_X \sim v_{\rm rot}^2$ scaling law (Pallavicini et al. 1981) we infer a magnetic field twice the strength of the solar one.

In order to explore the possibility that the planetary magnetosphere can directly affect the stellar coronal structure, we have conducted MHD simulations of a model of interacting magnetic fields with opposite alignment as in case A of Cohen et al. (2009). From these simulations, we infer that due to the relative motion of the planet and the star the global magnetic field is distorted and has an enhanced probability of reconnection events that can occur on the space between planet and star. Given the coupling of magnetic field and plasma, an enhanced plasma density is present around the planet and it forms a trail rotating synchronously with the planet. Globally, we find consistency between observations and predictions from MHD simulations, hinting that the overall activity could be enhanced by magnetic SPI. Hence, the age estimates of the system using activity indicators are suspect. Currently, the age of HD 189733 is estimated to be at least $\geqslant$0.6 Gyr. The M-type companion, HD 189733A, is not detected at a level of luminosity of $L_X < 10^{27}$ erg s^{-1}, thus suggesting an age for the system older than 1.7–2 Gyr.

We have also analyzed the spectrum of an X-ray source close to HD 189733 and brighter in 2007 than in 2009. The spectrum is quite hard and from best fit we derive an absorption of $N_{\rm H} \sim 1.4 \times 10^{21}$ cm^{-2} suggesting that this is an object in the Galaxy but quite distant from the Sun.

The *XMM* guest investigator program supported I.P. through grant NNX09AP46G. S.J.W. was supported by NASA contract NAS8-03060 to the Chandra Science Center. V.K. acknowledges CXC NASA contract NAS8-39073, and O.C. acknowledges NASA LWSTRT grant NNG05GM44G.

REFERENCES

Bakos, G. Á., Pál, A., Latham, D. W., Noyes, R. W., & Stefanik, R. P. 2006, ApJ, 641, L57
Bouchy, F., et al. 2005, A&A, 444, L15
Branduardi-Raymont, G., et al. 2007, A&A, 463, 761
Burrows, A., Budaj, J., & Hubeny, I. 2008, ApJ, 678, 1436
Cohen, O., Drake, J. J., Kashyap, V. L., Saar, S. H., Sokolov, I. V., Manchester, W. B., Hansen, K. C., & Gombosi, T. I. 2009, ApJ, 704, L85
Cutri, R. M., et al. 2003, VizieR Online Data Catalog, 2246, 0
Dickey, J. M., & Lockman, F. J. 1990, ARA&A, 28, 215
Feigelson, E. D., et al. 2004, ApJ, 611, 1107
Giardino, G., Pillitteri, I., Favata, F., & Micela, G. 2008, A&A, 490, 113
Henry, G. W., & Winn, J. N. 2008, AJ, 135, 68
Hui, Y., Schultz, D. R., Kharchenko, V. A., Stancil, P. C., Cravens, T. E., Lisse, C. M., & Dalgarno, A. 2009, ApJ, 702, L158
Kalberla, P. M. W., Burton, W. B., Hartmann, D., Arnal, E. M., Bajaja, E., Morras, R., & Pöppel, W. G. L. 2005, A&A, 440, 775
Kashyap, V. L., Drake, J. J., & Saar, S. H. 2008, ApJ, 687, 1339
Knutson, H. A. 2007, Nature, 448, 143
Lammer, H., Selsis, F., Ribas, I., Bauer, S. J., & Weiss, W. W. 2003, ApJ, 598, L121
Lanza, A. F. 2008, A&A, 487, 1163
Lanza, A. F. 2009, A&A, 505, 339
Liang, M.-C., Seager, S., Parkinson, C. D., Lee, A. Y.-T., & Yung, Y. L. 2004, ApJ, 605, L61
Linsky, J. L., Yang, H., France, K., Froning, C. S., Green, J. C., Stocke, J. T., & Osterman, S. N. 2010, ApJ, 717, 1291
Maggio, A., Flaccomio, E., Favata, F., Micela, G., Sciortino, S., Feigelson, E. D., & Getman, K. V. 2007, ApJ, 660, 1462
Mamajek, E. E., & Hillenbrand, L. A. 2008, ApJ, 687, 1264
Melo, C., Santos, N. C., Pont, F., Guillot, T., Israelian, G., Mayor, M., Queloz, D., & Udry, S. 2006, A&A, 460, 251
Montes, D., López-Santiago, J., Gálvez, M. C., Fernández-Figueroa, M. J., De Castro, E., & Cornide, M. 2001, MNRAS, 328, 45
Moutou, C., et al. 2007, A&A, 473, 651
Pallavicini, R., Golub, L., Rosner, R., Ayres, T., & Linsky, J. L. 1981, ApJ, 248, 279
Pont, F., et al. 2007, A&A, 476, 1347
Reale, F. 2007, A&A, 471, 271
Reale, F., Betta, R., Peres, G., Serio, S., & McTiernan, J. 1997, A&A, 325, 782
Reale, F., Güdel, M., Peres, G., & Audard, M. 2004, A&A, 416, 733
Serio, S., Reale, F., Jakimiec, J., Sylwester, B., & Sylwester, J. 1991, A&A, 241, 197
Shkolnik, E., Bohlender, D. A., Walker, G. A. H., & Collier Cameron, A. 2008, ApJ, 676, 628
Shkolnik, E., Walker, G. A. H., & Bohlender, D. A. 2003, ApJ, 597, 1092
Shkolnik, E., Walker, G. A. H., Bohlender, D. A., Gu, P., & Kürster, M. 2005, ApJ, 622, 1075
Winn, J. N., et al. 2006, ApJ, 653, L69
Zacharias, N., Monet, D. G., Levine, S. E., Urban, S. E., Gaume, R., & Wycoff, G. L. 2005, VizieR Online Data Catalog, 1297, 0